LAWRENCE
LIVERMORE
NATIONAL
LABORATORY

LLNL-JRNL-736260

Direct Ink Write Fabrication of Transparent Ceramic Gain Media

I. K. Jones, Z. M. Seeley, N. J. Cherepy, E. B. Duoss, S. A. Payne

August 7, 2017

Optical Materials

Disclaimer

This document was prepared as an account of work sponsored by an agency of the United States government. Neither the United States government nor Lawrence Livermore National Security, LLC, nor any of their employees makes any warranty, expressed or implied, or assumes any legal liability or responsibility for the accuracy, completeness, or usefulness of any information, apparatus, product, or process disclosed, or represents that its use would not infringe privately owned rights. Reference herein to any specific commercial product, process, or service by trade name, trademark, manufacturer, or otherwise does not necessarily constitute or imply its endorsement, recommendation, or favoring by the United States government or Lawrence Livermore National Security, LLC. The views and opinions of authors expressed herein do not necessarily state or reflect those of the United States government or Lawrence Livermore National Security, LLC, and shall not be used for advertising or product endorsement purposes.

Direct Ink Write Fabrication of Transparent Ceramic Gain Media

Ivy Krystal Jones, Zachary M. Seeley*, Nerine J. Cherepy, Eric B. Duoss, and Stephen A. Payne
Lawrence Livermore National Laboratory, Livermore, CA 94551

Abstract

Solid-state laser gain media based on the garnet structure with two spatially distinct but optically contiguous regions have been fabricated. Transparent gain media comprised of a central core of $Y_{2.97}Nd_{0.03}Al_{5.00}O_{12.00}$ (Nd:YAG) and an undoped cladding region of $Y_3Al_5O_{12}$ (YAG) and were fabricated by direct ink write and transparent ceramic processing. Direct ink write (DIW) was employed to form the green body, offering a general route to preparing functionally structured solid-state laser gain media. Fully-dense onerine ptical ceramics in a "top hat" geometry with YAG / Nd:YAG have been fabricated by DIW methods with optical scatter at 1064 nm of <3%/cm.

Keywords: (160.5690) Rare-earth-doped materials; (140.3580) Lasers, solid-state; (310.3840) Materials and process characterization; (220.4610) Optical fabrication

*Corresponding author.
E-mail address: seeley7@llnl.gov
Telephone: 925-423-0346
FAX: 925-423-6394

1. Introduction

Solid-state laser gain media has been dominated for over sixty years by single crystal growth methodology [1]. Over the last two decades, transparent ceramics have emerged as an alternative pathway for the fabrication of solid-state laser gain material with improved mechanical, thermal, and optical properties [2-5]. Transparent ceramics are being developed for various applications such as transparent armor, lighting fixtures, scintillators, IR windows and missile domes [6,7]. Advantages of transparent ceramics include their rugged mechanical properties due to their polycrystalline microstructure, formability with higher doping concentrations and better doping uniformity, since they are fabricated via sintering rather than from the melt, as well as the ability to manufacture complex and large contiguous shapes. Secondarily, these materials can be more cost effective in comparison to their single crystal counterparts, as they do not require slow solidification from the melt in order to provide large transparent boules. Transparent ceramics possess various advantages over conventional optically transparent materials such as glasses, in that they are crystalline – important for obtaining narrow spectroscopic linewidths with rare-earth dopants, such as Nd^{3+}. While single crystal and glass laser gain media are advanced and well-developed technologies, transparent ceramics offer functional opportunities not readily attainable with structures grown from the melt.

Previous efforts to produce structured ceramic laser gain media have relied on assembly of multiple layers at the green body stage [8-10]. In this contribution, we describe the fabrication of a Nd^{3+} dopant profile that is concentrated in the center of a Nd:YAG laser rod as a "top-hat" step profile, (or in the future as a smooth, graded profile), to increase the pump efficiency by a factor of 2x while stabilizing the desired laser mode profile in the transverse electromagnetic (TEM_{00}) mode. Ceramics processing enables the fabrication of a spatially-controlled chemical composition at the stage of green body fabrication, formed via direct ink write (DIW). We are using 3D DIW printing techniques [11-14] to fabricate compositionally-controlled green bodies, subsequently sintered to transparency for use as laser gain media.

As shown in Fig. 1a, a laser rod with a "top hat" Nd^{3+}-doped gain region, in principle, has built-in laser mode-control within the structure that better matches the TEM_{00} laser mode than a uniformly-doped Nd:YAG rod, while the TEM_{01} and other higher-order modes are not favored, since no Nd^{3+} dopant is present beyond 0.1 cm in the cladding region in this design. (The details of this standard laser calculation are summarized in the Appendix.) Fig. 1b shows that the predicted output power for the TEM_{00} mode in a Nd:YAG ceramic with a "top hat" dopant profile is favored, compared to the first higher order mode (TEM_{10}) shown for comparison, which has a higher threshold and a reduced slope efficiency. We note in passing that for a typical *highly multimode* laser, doped at 0.9 at.% and having a loss level of 0.3%/cm (which are typical specifications for commercial crystalline laser rods), the peak power at the design point is 2.27 kW at the circled design point on the Figure – which is only modestly higher than the modeled single-mode laser. A final issue to be addressed in the design of a practical "top hat" ceramic laser rod with a Nd-doped core or gradient involves the change in refractive index induced by the Nd doping of $\Delta n = 0.00043$/at.%, as reported by Zelmon et al. [15] and reproduced by us. At 2% Nd-doping, this would amount to 50 waves of distortion between the core and the clad for a 6 cm rod, which however can be compensated for by way of the addition of ~10% Lu-dopant to the "undoped" YAG region, (controlled to +/- 0.1% doping accuracy).

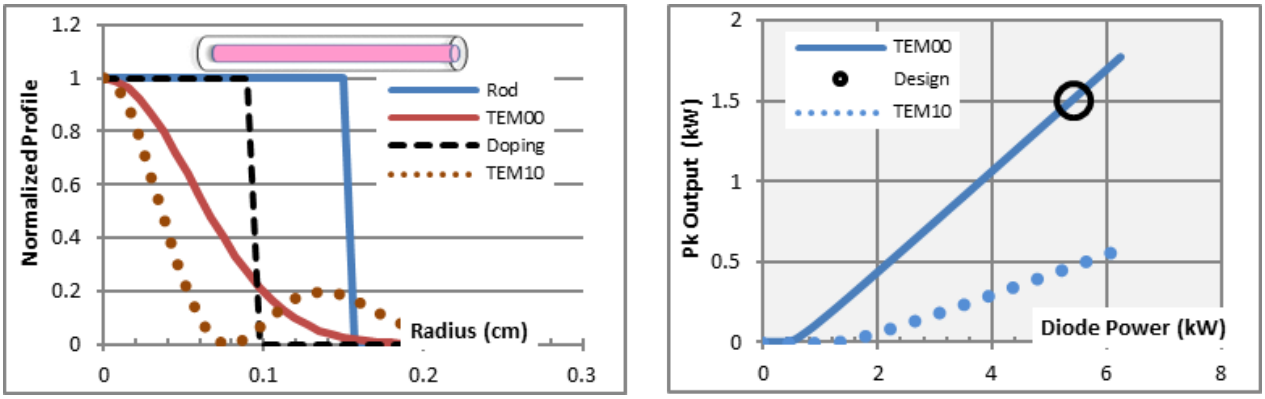

(a) **(b)**

Fig. 1. **(a)** Normalized profile of the rod radius (blue line), "top hat' doping profile (black dashed line), TEM_{00} intensity profile (red line), and TEM_{10} profile (red dots). **(b)** Peak output power as a function of pump diode power corresponding to the TEM_{00} laser mode (solid blue line), and TEM_{10} laser mode (blue dots).

Previous efforts to build optical structures with compositional gradients have involved assembling pressed and layered green bodies (Konoshima, Japan [16]) and using diffusion bonding to join carefully cut and polished single crystal optical components (Onyx Optics, Pleasanton, USA [17]). At LLNL, "top hat" laser rods with Nd^{3+}-doped core and undoped cladding have been fabricated via composite green body assembly (Fig. 2). However, radially-graded green bodies are difficult to prepare by this approach, as smooth gradients are not easily achieved. In this paper we report on our efforts to adapt DIW methods to the requirements for a functionally graded transparent ceramic.

(a) (b)

Fig. 2. "Top-hat" transparent ceramic with Nd^{3+} doped core and undoped cladding formed by green body assembly methods at LLNL **(a)** top-view and **(b)** side-view.

2. Experimental Procedure

2.1 Powder characterization

Fabrication of high quality, fully-dense and transparent optical ceramics requires high purity precursor powder. Nanoparticles with the compositions $Y_3Al_5O_{12}$ and $Y_{2.94}Nd_{0.06}Al_5O_{12}$ (YAG/YAG:Nd) were fabricated via flame spray pyrolysis (FSP) by Nanocerox and then calcined in air between 900 and 1200˚C. The morphology of the calcined YAG nanopowders were analyzed via bright-field transmission electron microscopy (TEM) using a FEI Titan 80-300 S/TEM with an operational voltage of 300 kV. X-ray diffraction (XRD) performed using the XRD-Bruker AXS D8 Advance, a Cu anode diffractometer ($K\alpha_1$ = 0.1540598 nm). The X-ray diffraction patterns were displayed via Bruker AXS EVA data acquisition software. The samples were prepared by dispersing the nanopowders onto silicon single crystal wafers with acetone using a step size of 0.059482 from 16° - 60° diffraction angle range. The surface area measurements of the YAG and Nd:YAG nanoparticles were determined by Brunauer, Emmett, and Teller (BET) analysis using a Micromeritics ASAP 2020 surface area and porosity analyzer.

2.2 Ink Preparation and Characterization

High purity ink components used for writing the green body were obtained from Sigma Aldrich, to ensure optimization of sintering processes [18]. The colloidal suspensions consisted of: nanopowder, YAG/Nd:YAG 30 – 60 vol% loading; an ether-based solvent 10 – 25 wt%; binder, poly(ethylene glycol) (PEG, weight-average molecular weight, M_w = 400 – 800 g mol^{-1}), 5 – 15 wt%; and an ether-derivatized carboxylic acid surfactant, 5 – 15 wt%. To achieve optimum dispersion and minimum agglomeration, the nanopowders were mixed using a high shear mixer, initially with surfactant to permit surface adsorption, rendering the metal oxide nanoparticles to be soluble. Surface-adsorbed carboxylate groups result in the chemical and physical alteration of the nanoparticles neutralizing negative and positive surface charges and coating with a tail of ether chemical structure. Inks were characterized for their rheological properties using an AR2000ex TA Instruments rotating disk rheometer.

2.3 Direct Ink Write

During the direct ink write (DIW) process, a high solids-loading nanoparticle ink (30-45 vol%) is extruded through a 500 μm nozzle and written into a structure that can be tuned in composition. Syringes filled with the nanoparticle inks were loaded onto a 3-axis micro-positioning stage (Aerotech). A constant pressure was used to deliver the inks through a 610 μm nozzle at a linear feed rate of 5 mm/s. Aerotech's G-code was used to direct the 3-axis stage in order to build a cylindrical structure layer by layer.

2.4 Ceramic Processing

Traditionally, transparent ceramics are formed by pressing, sintering and HIPing the nanoparticle feedstock to full density [19-24]. After the green structures were printed by DIW, they were dried in air at 100˚C. Green density was increased further by cold isostatic pressing at 200 MPa. The polymer binder system was burned away at 1000˚C in air, followed by vacuum

sintering in a tungsten element furnace at 1750˚C to achieve closed porosity at densities of approximately 97-99%. Finally, the sintered ceramics were hot isostatically pressed (HIP'ed) for 4 hr under 200 MPa argon pressure and 1750˚C to reach fully dense polycrystalline transparent ceramics. To inspect transparency, ceramic surfaces are ground and optically polished.

2.5 Optical Characterization

Optical scatterometry with an 8" integrating sphere was used for routine characterization of scatter loss in polished transparent ceramics. UV-visible absorption, fluorimetry, optical microscopy, scanning electron microscopy with EDX, and electron microprobe for positional elemental analysis, were employed to further characterize compositionally tuned transparent ceramics.

3. Results and Discussion

The precursor FSP nanopowder, analyzed by TEM, was found to be comprised of loosely agglomerated spherical particles with particle sizes ranging from 30 nm to 150 nm (Fig. 3). Upon calcination at higher temperatures above 900˚C, the powder begins to form harder agglomerates with some initial sintering and neck formation between particles.

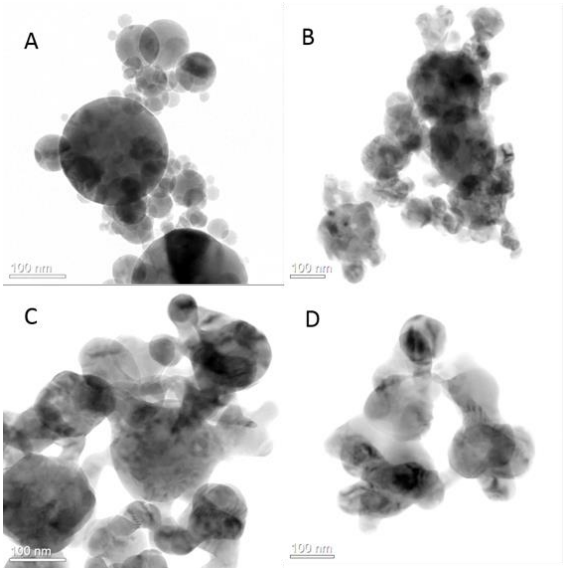

Fig. 3. Bright-field TE micrograph digital images of the morphology of calcined YAG nanopowders at different temperatures **(a)** 900°C for 5 hours in flowing air, **(b)** 1000°C for 1 hour in air, **(c)** 1100°C for 1 hour in air and **(d)** 1200°C for 1 hour in air.

X-ray diffraction (XRD) analysis was utilized for the identification of crystal phases present in the calcined powder (Fig. 4). Initially, after the 900˚C heat treatment, perovskite is the only observable crystalline phase. However, upon calcination at 1000˚C, the garnet phase starts to appear as the perovskite phase starts to diminish, and by 1100˚C the powder is fully transformed to garnet phase.

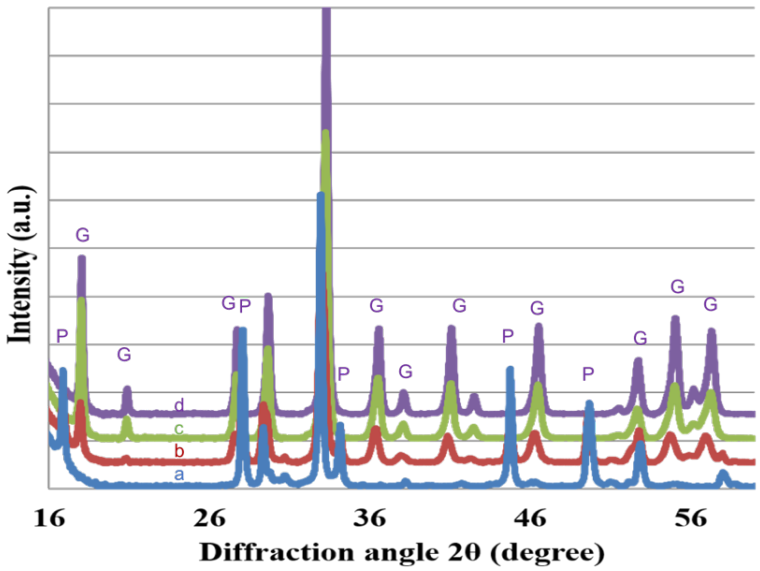

Fig. 4. XRD diffractograms displaying the crystal phases, Perovskite (P) and Garnet (G), of the calcined nanopowder of Nd:YAG (a) amorphous phase calcined at 900°C (blue), (b) amorphous and perovskite phase calcined at 1000°C (red), (c) perovskite and garnet phase calcined 1100°C (green) and (d) fully garnet phase calcined at 1200°C (purple).

The BET surface area analysis of this powder was also measured as a function of calcination temperature, see Table 1. Specific surface area was reduced with increasing calcination temperature. These results are consistent with the TEM images, indicating a significant amount of coarsening and agglomeration is occurring between 900 and 1200˚C.

Table 1. BET Surface Area Analysis of YAG and Nd:YAG Nanopowders.

Calcination (°C)	$Y_3Al_5O_{12}Y_{2.97}$ (m^2/g)	$Nd_{0.03}Al_5O_{12}$ (m^2/g)
900	17.6	22.7
1000	13.5	18.3
1100	11.8	12.9
1200	10.5	12.6

For optimal ceramic densification during sintering, small primary particles with minimal agglomeration and high surface area are preferred. However, the as-synthesized powder exhibits mainly perovskite phase, which must transform to garnet. If this phase transition occurs after the green body stage, cracking in the ceramics may result. Therefore, in this study, powder was calcined at 1100°C in order to crystallize it as garnet phase prior to formulation into inks.

The calcined powders were mixed with the optimal ratio of surfactant, solvent, and binder to create high solids-loading inks. In order to enable printing of a green structure, the viscosity and shear thinning characteristics of the ink was optimized. Fig. 5 shows a typical ink used for fabrication of the green bodies shown here. It offers significant shear-thinning (decrease in viscosity at high shear rates) that allows the green bodies to be printed quickly and uniformly, along with high viscosity at low shear rates that allows the green body to retain its form after printing. The viscoelastic response of the material spans two orders of magnitude, allowing for high flow-rate printing through the nozzle, and shape retention after extrusion.

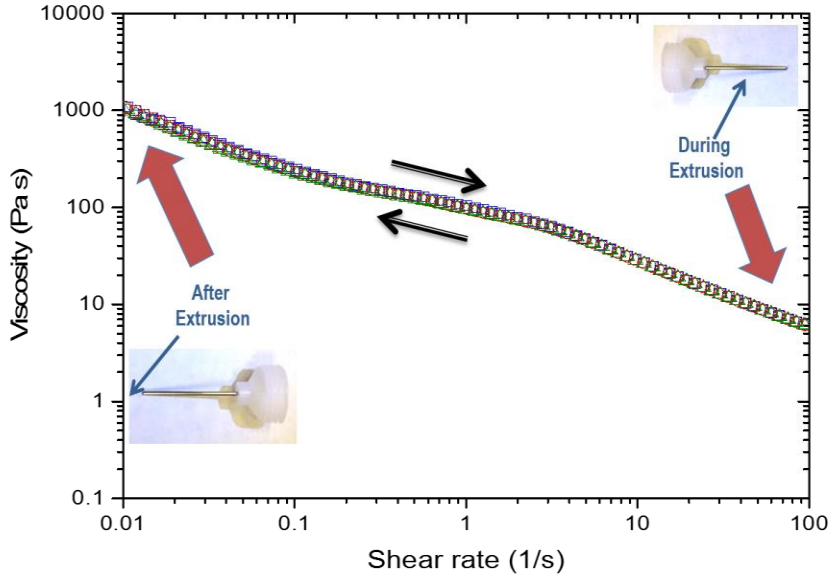

Fig. 5. Viscosity vs. shear rate reveals strong shear thinning of the ink used, and high viscosity at low shear.

The DIW method is based on the continuous deposition of YAG nanopowder-based slurry, extruded in a layer-wise fashion to build up a structure controlled in radial and longitudinal composition. Examples of DIW green bodies are shown in Fig. 6 (a) and (b).

(a) (b)

Fig. 6. Two green bodies fabricated via DIW (a) undoped YAG and (b) "top-hat" with Nd^{3+}-doped core and undoped cladding.

The 3D-printed green structures are step-wise densified via pressure and/or temperature [19-21]. Fig. 7 shows the densification steps and images of a ceramic at each step. Tap density of the nanopowder starts off at ~5%. This powder is made into an ink with ~45 vol.% solids loading and printed into a 45% dense green structure. After cold isostatic pressing the structure at 200 MPa, it reaches ~55% dense. After vacuum sintering at 1750˚C, the ceramics reach densities of ~99%, with closed porosity. Finally, the remaining pores are pressed out via the HIP step at 1750˚C and 200 MPa argon pressure resulting in fully dense transparent ceramic optics. Fig. 8 shows close-up images of a DIW-fabricated ceramic with an Nd-doped core and an undoped cladding through the process steps of green, sintered, and HIP'ed structure.

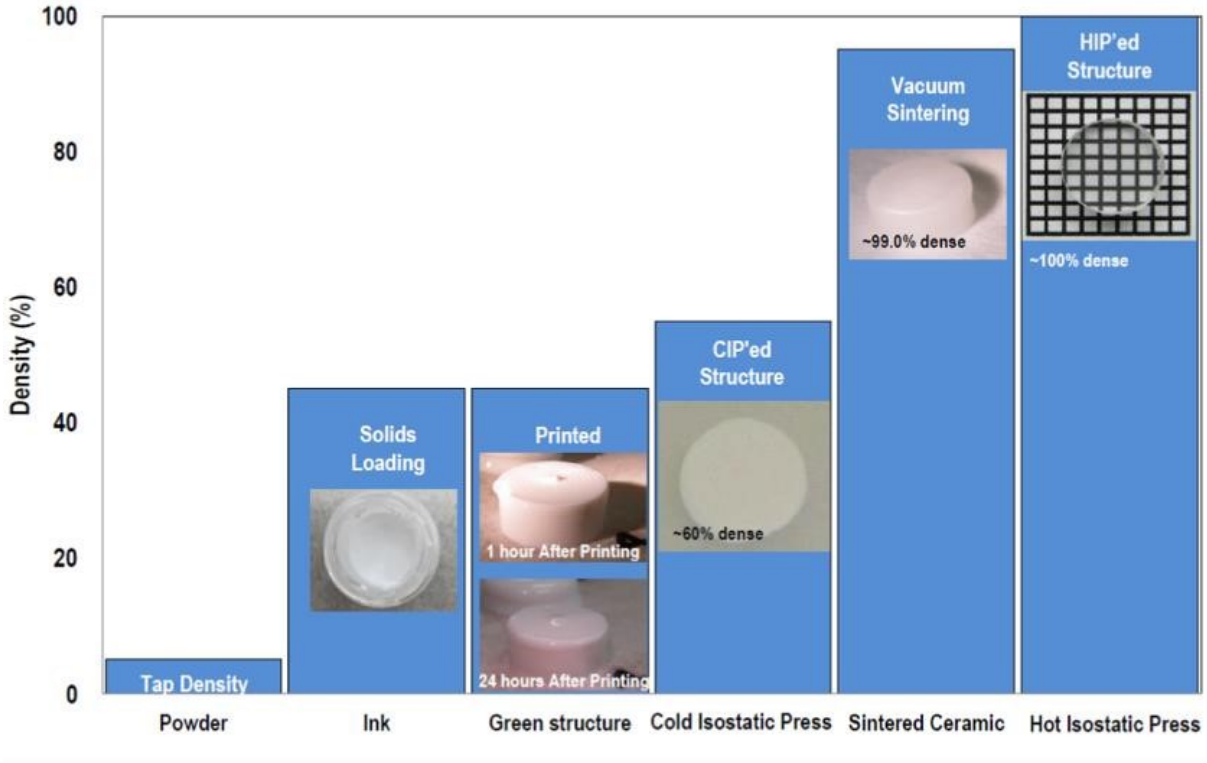

Fig. 7. Densification during transparent ceramic processing steps.

Fig. 8. (a) DIW green body structure of YAG, (b) vacuum-sintered DIW structure of YAG, and (c) hot isostatically pressed, fully-dense DIW structure of YAG/Nd:YAG.

In order to characterize the profile of the interface between the Nd:YAG and YAG cladding, we used an electron microprobe to analyze the concentration of neodymium in a top-hat profile ceramic. Fig. 9 shows the concentration of Nd/Y as a function of the distance across the diameter of the ceramic. The outside 2 mm of the ceramic is the un-doped YAG cladding, and the 1% Nd-doped YAG core has a ~8 mm diameter. The inset graph in the center of Fig. 9 shows the interface at a higher resolution, revealing that the concentration of Nd goes from 0 to 1% in approximately 70 microns. This indicates that during the fabrication process Nd is diffusing somewhat across the interface into the undoped cladding. This could be occurring during the printing stage when the ink is still wet, or by solid state diffusion during the high processing temperature steps. This distance is consistent with solid state diffusion, reported in previous studies of doped transparent ceramics [22].

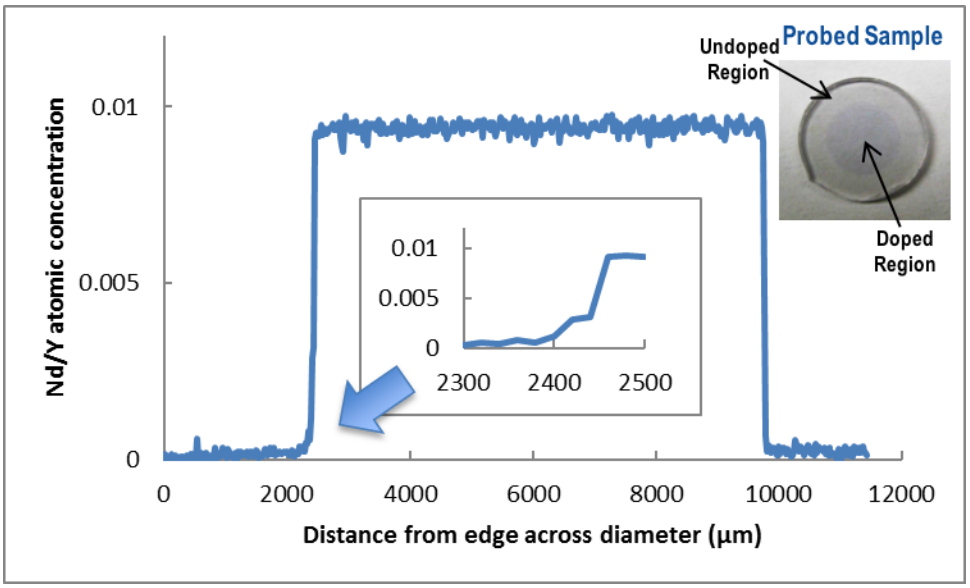

Fig. 9. Concentration of neodymium ions across the diameter of a core/clad top-hat profile measured by electron microprobe. Inset shows the left interface region at higher resolution.

Most laser cavities are designed to accommodate laser rods with a high aspect ratio geometry, a common size being ~5 mm diameter and ~6 cm in length. This aspect ratio is difficult to print, but with the help of a support structure we have thus far printed a 2 cm tall core/clad "top-hat" profile transparent laser rod shown in Fig. 10, and have printed green structures up to 7 cm tall.

We have achieved optical scatter of 1%/cm at 1064 nm in printed transparent ceramics for single-ink structures, and expect that, while challenging, the reliable production of low-loss gain media via these methods will be possible [23,24].

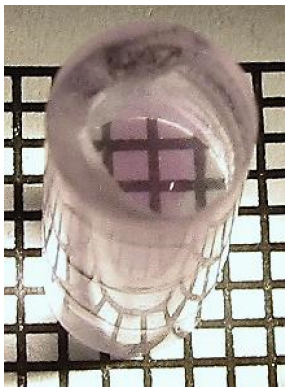

Fig. 10. Top view of a 2 cm tall by 4 mm diameter DIW printed core/clad "top-hat" profile transparent ceramic laser rod with 2 at.% Nd doping in the core region. Optical scatter was measured through the core to be <3%/cm at 1064 nm.

4. Summary

Building on prior laser research which have recognized the value of graded doping for enhanced performance [8-10,25,26], we have shown that transparent ceramics formed from direct ink written green bodies is a viable approach to produce optics with advantageous doping profiles not attainable by melt-growth single crystals. Optimizing the powder properties and ink viscosity is important for enabling the printing of a robust green structure which is able to be sintered to high transparency. The technique can be exercised with a two-nozzle system to write doped and undoped regions into an optic, and the geometry stays intact through the sintering steps to the final optic. In the future, we are planning to deploy a mixing chamber to construct smooth compositionally-graded structures using two inks with a single nozzle.

5. Appendix

One future pathway for gain elements fabricated by DIW entails laser rods having both doped and undoped regions. This design mimics, in a sense, the advantages of mode-control afforded by the laser-pumped laser configuration. We developed a model to describe laser rods with Nd-doped core and undoped clad regions, based on the following [27-29]:

- Using standard analytical methods of mode-matching based on overlap functions of the pumped region with the cavity mode, (which is presumed specified by optics external to the laser rod)
- Modeling the case of the Cutting Edge Optronics (CEO) RBAT 30-3P laser head pumped by up to 5.4 kW of peak diode power, employing 250 μsec pulses with a 6.3 cm long laser rod, and benchmarking the pumping efficiency to the diode-side-pumped multi-pass geometry reported by CEO

- Accounting for optical losses at the laser wavelength in terms of its impact on the laser threshold and slope efficiency, as well as the impact of the Nd lifetime (storage time) dependence on the doping level
- Using the following specific parameters to model the doped-core/undoped-clad rod laser: 1.8 mm diameter core region doped at 2 at.% Nd with a top hat profile, TEM_{00} mode radius of 1.1 mm, rod scatter loss of 1%/cm, output coupling of 60%, and an outer rod diameter of 3.0 mm.

Acknowledgements

We would like to thank Rebecca Dylla-Spears, Christopher Spadaccini, Cheng Zhu, Tim Yee, Ted Baumann, Zurong Dai, Adam Jaycox, Du Nguyen, Alexandra Golobic, Rick Ryerson and Nikola Dudukovic for helpful discussions and advice, experimental assistance and measurements. This work was sponsored by the LLNL LDRD program, under project designation LDRD 16-SI-03 and performed under the auspices of the U. S. Department of Energy by Lawrence Livermore National Laboratory under contract DE-AC52-07NA27344.

References

1. A.A. Kaminskii, Laser Crystals: Their Physics and Properties, Springer, (2013).
2. V. Lupei and A .Lupei, "Nd:YAG at its 50th anniversary: Still to learn" J. Luminesc., **169**, 426–439, (2016).
3. A. Ikesue, and Y.L. Aung, "Ceramic laser materials", Nat Photon **2**, 721-727, (2008).
4. J. Li, Y. Pan, Y. Zeng, W. Liu, B. Jiang, and J. Guo, "The history, development, and future prospects for laser ceramics: A review", Int. J. Refract. Met. H. **39**, 44-52, (2013).
5. J. Sanghera, W. Kim, G. Villalobos, B. Shaw, C. Baker, J. Frantz, B. Sadowski, I. Aggarwal, "Ceramic laser materials: Past and present", Opt. Mater., **35**(4), 693-699, (2013).
6. S.F. Wang, J. Zhang, D.W. Luo, F. Gu, D.Y. Tang, Z.L. Dong, G.E.B. Tan, W.X. Que, T.S. Zhang, S. Li, L.B. Kong, "Transparent ceramics: Processing, materials and applications," Prog. Solid State Chem. **41**, 20-54, (2013).
7. A. Goldstein and A. Krell, "Transparent Ceramics at 50: Progress Made and Further Prospects," J. Am. Ceram. Soc., **99** (10) 3173–3197, (2016).
8. F. Tang, Y. G. Cao, J. Q. Huang, W. Guo, H. G. Liu, W. C. Wang, Q. F. Huang and J. T. Li, "Diode-pumped multilayer Yb:YAG composite ceramic laser," Laser Phys. Lett., **9**, 564, (2012).
9. L. Esposito, J. Hostasa, A. Piancastelli, G. Toci, D. Alderighi, M. Vannini, T. Epicier, A. Malchere, G. Alombert-Goget and G. Boulon, "Multilayered YAG-Yb:YAG ceramics: manufacture and laser performance," J. Mater. Chem. C, **2**, 10138, (2014).
10. H. Rao, Zh. Liu, Zh. Cong, Q. Huang, Y. Liu, S. Zhang, X. Zhang, Ch. Feng, Q. Wang, L. Ge and J. Li, "High power YAG/Nd:YAG/YAG ceramic planar waveguide laser," Laser Phys. Lett. **14**, 045801, (2017).
11. J. Deckers, J. Vleugels, J.-P. Kruth, "Additive Manufacturing of Ceramics: A Review", J. Ceram. Sci. Tech. **05** (04), 245-260, (2014).
12. J. Lewis, "Direct Ink Writing of 3D Functional Materials", Adv. Funct. Mater., **16** (17), 2193-2204, (2006).

13. K.K.B. Hon, L. Li, I.M. Hutchings, "Direct writing technology – Advances and developments", CIRP Ann Manuf Technol **57** (2), 601-620, (2008).
14. N. Travitsky, A. Bonet, B. Dermeik, T. Fey, I. Filbert-Demut, L. Schlier, T. Schlordt, and P. Greil, "Additive Manufacturing of Ceramic-Based Materials", Adv. Eng Mater **16** (6), 729-754, (2014).
15. D. E.Zelmon, K. L. Schepler, S. Guha, D. Rush, S. M. Hegde, L. P. Gonzalez and J. Lee, "Optical properties of Nd-doped ceramic yttrium aluminum garnet", Laser-Induced Damage in Optical Materials: 2004, edited by G. J. Exarhos, et al., Proceedings of SPIE Vol. 5647 (2004).
16. http://www.konoshima.co.jp/eng/ceramics/feature.html
17. http://www.onyxoptics.com/products/standard.php
18. J.E. Smay, J. Cesarano, and J.A. Lewis, "Colloidal Inks for Directed Assembly of 3-D Periodic Structures," Langmuir **18** (14), 5429-5437, (2002).
19. Z.M. Seeley, N.J. Cherepy, and S.A. Payne, "Expanded phase stability of Gd-based garnet transparent ceramic scintillators," J. Mater. Res. **29** (19), 2332-2337, (2014).
20. Z.M. Seeley, N.J. Cherepy, and S.A. Payne, "Homogeneity of Gd-based garnet transparent ceramic scintillators for gamma spectroscopy", J Cryst Growth **379**, 79-83, (2013).
21. Z.M. Seeley, N.J. Cherepy, and S.A. Payne, Two-step sintering of $Gd_{0.3}Lu_{1.6}Eu_{0.1}O_3$ transparent ceramic scintillator," Opt. Mater. Express **3** (7), 908-912, (2013).
22. C. Ma, F. Tang, J. Zhu, Z. Wen, Y. Yu, K. Wang, M. Du, J. Zhang, J. Long, X. Yuan, W. Guo, Y. Cao, "Cation diffusion at the interface of composite YAG/RE:LuAG (RE+Nd or Yb) transparent ceramics," J Eur. Ceram. Soc. 36 (10), 2555-2564, (2016).
23. Ikesue, K. Yoshida, T. Yamamoto, I. Yamaga, "Optical scattering centers in polycrystalline Nd:YAG Laser", J. Am. Ceram. Soc. **80** (6), 1517-1522 (1997).
24. R. Boulesteix, A. Maître, J.-F. Baumard, Y. Rabinovitch, F. Reynaud, "Light scattering by pores in transparent Nd:YAG ceramics for lasers: correlations between microstructure and optical properties", Opt Express **18** (14), 14992-15002, (2010).
25. P. Ferrara, M. Ciofini, L. Esposito, J. Hostaša, L. Lapucci, A. Pirri, G. Toci, M. Vannini, L. A. Gizzi, "3-D numerical simulation of Yb:YAG active slabs with longitudinal doping gradient for thermal load effects assessment", Opt. Express **22** (5), 5375-5386, (2014).
26. G. Bourdet, C. Gouedard, "Theoretical analysis of an end-pumped Yb:YAG active mirror thin-disk amplifier with a longitudinal doping concentration gradient", Appl. Opt. **53** (31), 7556-7565, (2014).
27. G. Shayeganrad, "Efficient design considerations for end-pumped solid-state-lasers", Opt. Laser Technol. **44** (4), 987–994, (2012).
28. Information on the laser head derived from the Northrop Grumman Cutting Edge Optronics web site, http://catalog.cuttingedgeoptronics.com/item/laser-modules/laser-gain-modules/rbat30-3p, and further details were obtained from George Doster at CEO.
29. D. C. Brown, "Heat, fluorescence, and stimulated-emission power densities and fraction in Nd:YAG", IEEE Journal of Quantum Electronics **34** (3), 560-572, (1998).